Rapid Measurement of Magnetic Particle Concentrations in Wildland-Urban Interface Fire Ashes and Runoff Using Compact NMR

Jacob S. Martin, Austin R.J. Downey, Mohammed Baalousha, and Sang Hee Won

***Abstract*— Wildfires are increasing in size, frequency, and intensity, releasing increased amounts of contaminants, including magnetic particles, into the surrounding environment. The aim of this paper is to develop a sensing method for the detection and quantification of magnetic particles (MPs) in fire ash and fire runoff using a compact Time-Domain Nuclear Magnetic Resonance (TD-NMR) system. The system is made up of custom NMR electronics with a compact and rugged permanent magnet array designed to enable future deployment as an in situ sensor. A signal-to-noise ratio of 25 dB was measured for a single scan, and sufficient data can be acquired in one minute. A linear relationship with an R^2 value of 0.9699 was established between transverse relaxation rates and MP concentrations in ash samples. This was validated by testing known dilutions of pure magnetite particles and showing that they fit within the same linear curve. The developed approach was then applied to detect MPs in surface water, where changes in the relaxation rates as high as 400% were observed before and after a wildfire event. MPs were removed from the surface water using a magnetic particle separator to confirm that observed changes were solely due to the presence of MPs. The compact NMR system can be used as a simple and rapid approach to track and quantify the concentrations of magnetic particles released from fire ashes and also from other sources such as discharges from coal ash and other combustion ashes.**

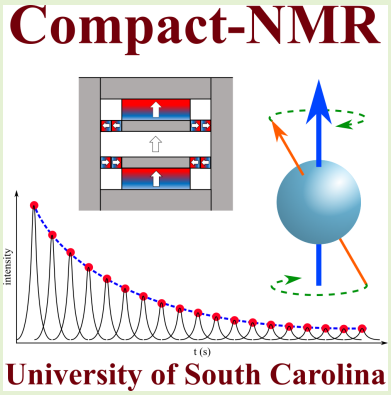

***Index Terms*— ash, magnetic particle, nuclear magnetic resonance, permanent magnet, in situ sensing, wildfire**

I. Introduction

NUCLEAR Magnetic Resonance (NMR) systems are highly useful devices that can provide rapid and non-destructive characterization of materials and typically require a minimal amount of sample preparation [2]. The most widely used NMR techniques utilize Fourier analysis to obtain high-resolution information about the molecular structures contained within a sample [3]. However, a very high magnetic strength and homogeneity is required to produce usable data for this technique. Most modern systems employ the use of large superconductors with cryogenic cooling to achieve necessary magnetic field conditions [4]. Although they are effective for highly sensitive molecular characterization, Fourier transform NMR systems are expensive and impractical to design at compact scales. This is why spectroscopy is used to analyze complex substances with many intermolecular interactions and is used for applications in drug identification, complex fuel analysis, and MRI systems [5], [6]. NMR relaxometry is an alternative, low-sensitivity technique with fewer requirements on the magnetic field and focuses on the relaxation processes in a material as a function of time rather than frequency [7]. Constant advancements in the quality and size of electronics, combined with the less stringent requirements for NMR relaxometry, allow for the ability to design simple, compact time-domain NMR (TD-NMR) systems that can be tailored to specific applications [8]. Although proton NMR techniques are most commonly used to analyze the molecular structures directly attached to the excited hydrogen nuclei, relaxometry can be used to obtain information about the environment that surrounds the excited

Manuscript received January 31, 2023; revised March 30, 2023. This material was sponsored by the ARO under Grant Number: W911NF-21-1-0306, the National Science Foundation under Grant No. 2101983 and the University of South Carolina under Grant No. 80004440. The views and conclusions contained in this document are those of the authors and should not be interpreted as representing the official policies, either expressed or implied, of ARO, NSF or the U.S. Government. The U.S. Government is authorized to reproduce and distribute reprints for Government purposes notwithstanding any copyright notation herein. An earlier version of this paper was presented at the 2022 IEEE Sensors Conference and was published in its Proceedings: https://doi.org/10.1109/SENSORS52175.2022.9967041

Jacob S. Martin is with the Department of Physics & Astronomy, College of Arts and Sciences and the Department of Mechanical Engineering, College of Engineering and Computing, at the University of South Carolina, Columbia, SC 29208 USA (e-mail: jsmartin@email.sc.edu).

Austin Downey and Sang Hee Won are with the Department of Mechanical Engineering, College of Engineering and Computing, at the University of South Carolina, Columbia, SC 29208 USA (e-mail: austindowney@sc.edu; sanghee@mailbox.sc.edu).

Mohammed Baalousha is with the Department of Environmental Health Sciences, Arnold School of Public Health, at the University of South Carolina, Columbia, SC 29208 USA (e-mail: mbaalous@mailbox.sc.edu).

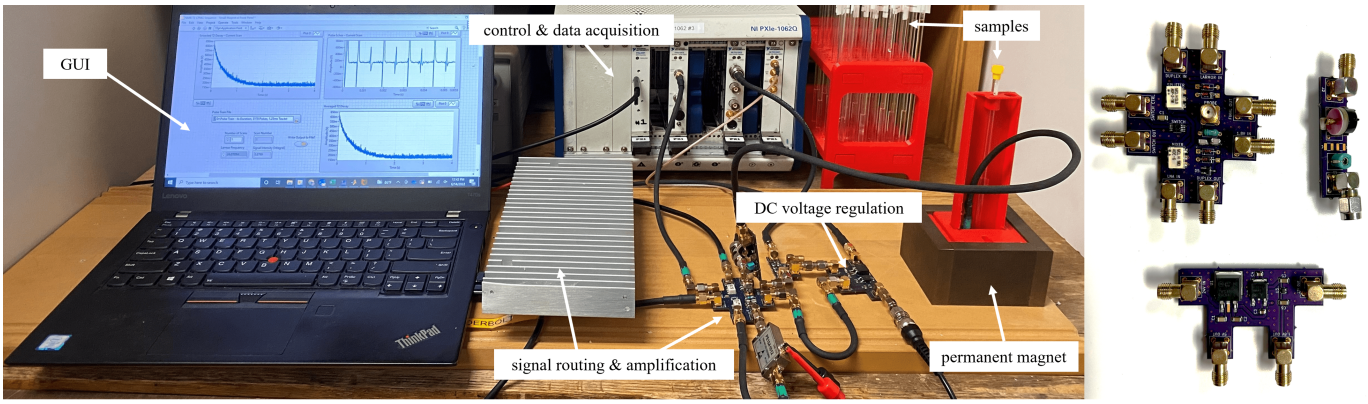

Fig. 1. (a) Full setup for the TD-NMR system, with key components and subsystems annotated and; (b) a close up view of the signal routing, tuning, and voltage regulation PCBs. [1]

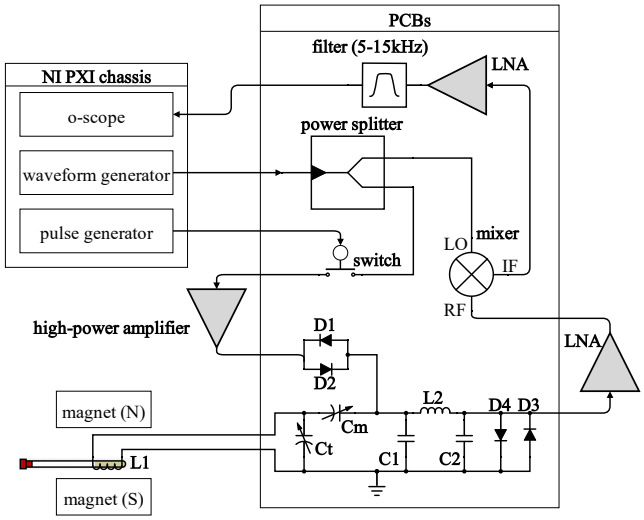

Fig. 2. Full schematic for the TD-NMR system, showing relevant components involved in the signal processing and amplification [1].

protons [9]. This typically manifests as a perturbation of the rate at which the signal of excited protons decays after being energized, otherwise known as the longitudinal and transverse (R_1 and R_2) relaxation rates. One possibility for employing this phenomenon for real-world applications is detecting the presence of magnetic particles (MPs). Magnetic particles alter the relaxation rate of nuclear spins by introducing small local magnetic fields near the protons that cause the R_2 rate to increase. MPs are a very powerful tool in the scope of NMR applications due to their ability to alter R_2 rates, and they are widely used as signal transducers in biosensing applications and as contrast agents in magnetic resonance imaging (MRI) studies [10]–[12]. Furthermore, it has been shown that shifts in water relaxivity have a direct linear correlation with the concentration of MPs in the water [13], [14].

While MPs are exceedingly effective in biomedical NMR applications, the usefulness of NMR systems for detecting MPs can be extended to the realm of environmental sensing. One utilization is the quantification of magnetic contents contained in wildfire ash and the detection of MPs in natural streams or bodies of water. Fires are a large cause of erosion and sediment transportation, and runoff is also increased as a result of intense fires. Another major impact of fires on sediment delivery is the movement of ash into streams and nearby bodies of water, which can have significant effects on water quality [15]. Fires have become more destructive in the western United States, and they are often spreading to areas with populations living in close proximity to wildland vegetation. This is known as the wildland-urban interface (WUI) [16]. Due to the rapid growth of regions that qualify as the WUI, as well as climate and societal changes, fire activity at the WUI is projected to increase globally. The increased emission of contaminants from wildland and WUI fires threatens ecosystems with air and water pollution and pose related problems for human health, so an understanding of the impacts of wildfires is more important than ever [17], [18].

Iron-bearing particles that exist in fire ash, specifically magnetite, have major effects on human health. Studies have suggested that airborne magnetite nanoparticles in the atmosphere may be able to enter the respiratory system or even brain tissue, and their presence has been linked to neurodegenerative diseases such as Alzheimer's and Parkinson's diseases [19]. Magnetite particles can also have environmental impacts such as promoting algal bloom formations and contributing to climate change through the absorption of solar radiation. Under the WUI fire conditions iron oxide particles undergo reduction (e.g., F3+ to Fe2+ to Fe0) resulting in the formation of magnetic particles such as maghemite, magnetite, and zero-valent iron [19]. The detection and quantification of these magnetic particles often require sophisticated approaches such as x-ray absorption spectroscopy using synchrotron radiation which is time-consuming and requires access to synchrotron facilities. Other known methods to detect MPs are superconducting quantum interference (SQUID) devices, atomic magnetometers, and spintronic devices such as giant magnetoresistance (GMR) sensors and tunneling magnetoresistance (TMR) sensors [10]. While effective, these devices are tailored for specific particle sizes and often restricted to surface-based

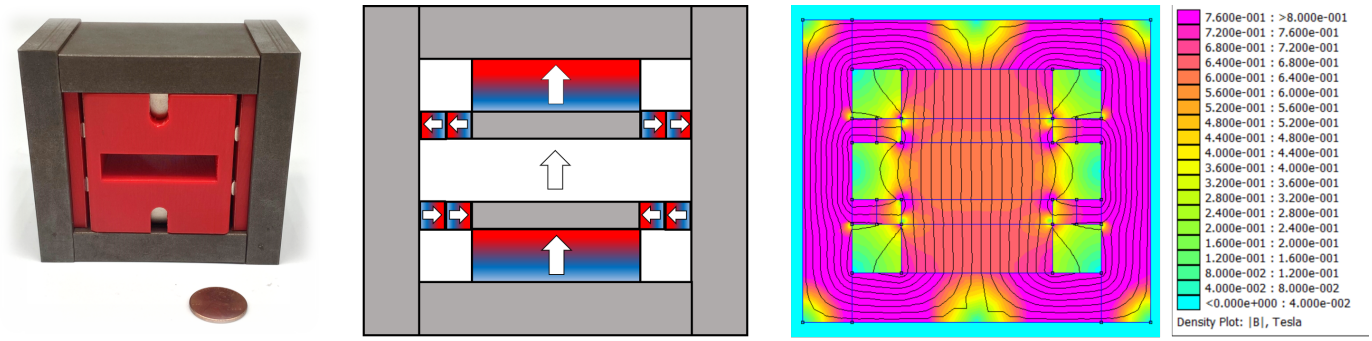

(a) (b) (c)

Fig. 3. The magnet array, showing: (a) fully assembled magnet; (b) orientation of individual magnets and steel pieces, and; (c) two-dimensional finite element simulation [1].

techniques. NMR allows for volumetric measurements and has no restrictions on particle sizes. This is a requirement since MP sizes in ash and surface water span from nano- to micro-scales [10]. In addition to ash measurements, assessing water samples from nearby bodies of water is also important. A storm following a fire event will transport large amounts of sediment and ash into surface water and rapid measurements can help to understand how widespread the effects of a fire are [20], [21]. Furthermore, a system capable of rapidly assessing magnetic ash content and also compact enough to perform in situ monitoring of natural water sources could be exceptionally useful.

Here we present a compact TD-NMR system capable of assessing the MP concentrations in wildfire ash and in surface water affected by runoff from wildfires. The system can perform fast, non-destructive tests that can be carried out with standard 5 mm tube sizes. A signal-to-noise ratio (SNR) of 25 dB was measured for a single scan. The prior publication for this work focused solely on identifying a linear relationship between the MP concentration and R_2 rate for a set of 10 ash samples. This work extends those findings to include a larger sample set of ashes, as well as the results of collecting and testing 10 surface water samples collected from twp inlets to Lake Madrone that were subjected to runoff following the North Complex Fire in California [19]. The linear relationship previously observed with the ash samples was verified to be accurate for quantifying MP concentrations by testing known dilutions of pure magnetite suspended in water. The linear curve has an R^2 value of 0.9699, making it a valid tool for quantifying MP concentrations in ash. For the runoff water testing, a magnetic particle separator was used in order to extract water from the runoff samples that was free of any MPs. This verified that the 100% and 400% increase in relaxation rates observed in the two inlets were due solely to the presence of MPs and not any other unknown environmental factors.

II. System Design

The full compact TD-NMR system is shown in Fig. 1 and a schematic for the electronics and control system is displayed in Fig. 2. A LabVIEW program is used for generating the necessary waveforms, calibrating to the optimal Larmor frequency, and collecting and exporting the final data. The laptop is connected to a NI PXI chassis by a Thunderbolt cable. The rest of the custom electronics are attached to the PXI chassis via 50 Ω cables. PCBs are used to mount all amplification and signal routing devices, except for the first stage low-noise amplifier (LNA) and the high-power amplifier. The probe is designed to be used with 5 mm diameter NMR tubes, which is a standard size for NMR applications.

A. Signal processing & Amplification Electronics

The primary electronics used for excitation and detection of the NMR signal are shown in Fig. 2. The system requires a single 24 V power supply, which is directed into a network of simple linear regulators that step the 24 V potential down to 12 V for the first stage LNA, 5 V for the second stage LNA, and 1.8 V for the switch. Excitation begins with a -5 dBm sinusoid driven from the waveform generator at the optimal Larmor frequency into a 2-way, 0° power divider. The sinusoid is split between the LO port of a frequency mixer with 4.6 dB conversion loss and an absorptive switch with 50 Ω terminated shunt legs. The switch state is controlled by the pulse generator, which is timed according to the Carr-Purcell-Meiboom-Gill pulse sequence to produce the RF pulses as needed [22]. The pulsed RF train is then sent to the high-power amplifier, which increases the power to 35 dBm. The high-power pulses are driven into the duplexer circuit, which is made up of a pi filter and crossed diodes. The duplexer, designed with lumped elements to match the Larmor frequency, blocks the large power pulses from damaging the LNA and isolates the majority of the power to the probe [23]. The probe is made up of a solenoidal coil and two adjustable tuning and matching capacitors. The hand-made solenoid is composed of 8 turns of Kapton insulated copper wire and has an inner diameter of 5 mm. Using the ceramic trimmer capacitors, one attached in series with the coil and one in parallel, the probe can be tuned and matched to 50 Ω. This is crucial to ensure that power delivery to the sample is maximized and reflections are minimal, as both can negatively affect the ability to read a clear signal if not optimized. The probe Q value, which is important for ensuring efficient power delivery to the coil, was calculated using the following:

$$Q = \frac{f_c}{\Delta f} \tag{1}$$

where f_c is the resonant frequency of the circuit, and Δf is the resonance width at half power [24]. The Q value for this probe was determined to be 70, which is large enough to provide efficient power delivery, but not so high as to make frequency optimization difficult when preparing to run a scan. Following the sample excitation, the microvolt-level NMR response travels through the duplexer and is amplified at the first stage LNA by 40 dB. This signal is then frequency-mixed with the original sinusoid to produce a decaying wave that lies within the range of audio frequencies. This makes the last stage of amplification simpler, as it is amplified again by 40 dB and filtered from 5-15 kHz using an operational amplifier as an active band pass filter.

B. Permanent Magnet Array

Contrary to MRI and NMR spectroscopy, there are very few demands on field homogeneity for relaxation and diffusion measurements [25]. This makes the permanent magnet design somewhat easier, but the field must still be sufficiently strong and homogeneous to produce stable, clear, and repeatable results. For this system a permanent magnet design was used that incorporates ten grade N42 NdFeB permanent magnets. The magnet design and final assembly can be seen in Fig. 3. Two 1.5 × 1.5 × 0.5 in thick magnets and eight 1.5 × 0.25 × 0.25 in thick magnets were used. 0.5 in thick 1018 carbon steel bars surround the magnet to create a return path for the magnetic flux, which greatly increases overall strength and safety by confining the majority of the field within its volume. There are also 0.25 in thick square steel caps placed on the magnet faces to provide an additional increase to the field homogeneity in the gap [26], [27]. Finite Element Method Magnetics was used to estimate the field before final assembly took place, shown in Fig. 3(c) [28]. Although the eight 0.5 in thick magnets are arranged with polarization perpendicular to that of the primary magnet blocks, they help to provide extra return paths for the magnetic flux and boost the overall strength inside the gap. The field magnitude showed a 30% increase when simulated with and without the eight blocks added and there was no change in homogeneity within the gap. The magnet was designed to be compact while still allowing for the use of 5mm sample tube sizes and to be exceptionally strong while still being safe. The ability to boost the field strength is crucial to the magnet design as the SNR for an NMR signal is proportional to the following factors:

$$\mathrm{SNR} \propto N\, A\, T^{-1}\, B_0^{3/2}\, \gamma_{\mathrm{exc}}\, \gamma_{\mathrm{obs}}^{3/2}\, T_2^{*}\, n_s^{1/2} \tag{2}$$

where N is the number of molecules, A represents the abundance of active spins, T is temperature, B_0 is the static magnetic field strength, γ_{exc} and γ_{obs} are the gyromagnetic ratios of the excited and observed spins, T_2^* is the effective transverse relaxation time (which is the inverse of relaxation rate), and n_s is the number of averages for a sample [29], [30]. The design is also cost-effective and easy to reproduce. To make the assembly process simpler and the overall design more secure, 3D-printed pieces were made to guide the pieces to their final locations. The room temperature field strength inside the gap was measured to be 0.565 T, and the Larmor frequency can be calculated from the following:

$$\omega = \gamma B_0 \tag{3}$$

where ω represents the Larmor frequency, B_0 is the static magnetic field strength in T, and γ is the gyromagnetic ratio, which has a value of 42.58 MHz/T. This indicates that the system will operate at about 24 MHz. A DC gaussmeter was used to measure a field homogeneity of 150 ppm over the sample volume. Although this is higher than most conventional NMR magnets, the fully assembled 2 kg magnet is compact, robust, easy to assemble, and sufficiently homogeneous for the measurements the system must perform. The magnetic field inhomogeneity for this magnet is estimated to be about 390 ppm [26]. If the field inhomogeneity were to be above 1500 ppm there would be too much spin decoherence within the sample volume and the output signal would be unobservable.

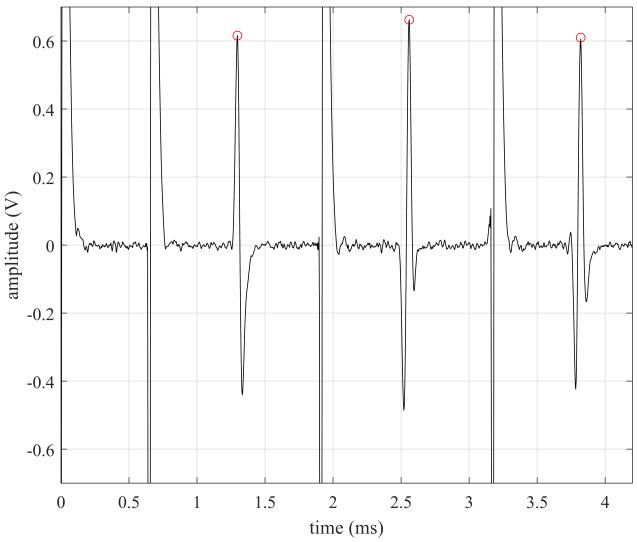

Fig. 4. Spin echos from a sample of MQ water following the application of a CPMG pulse sequence with a tau of 0.625 ms. The peak point (circled above) of each echo is collected to build the full transverse decay curve.

C. Signal Generation, Control, & Data Acquisition

The NI PXI chassis contains a pulse train generator, an arbitrary waveform generator, and a 16-bit digitizer that make up the signal generation, control, and data acquisition subsystems. A LabVIEW program controls the timing of the waveforms; the rising edge of the pulse train generator triggers the switch as well as the sinusoid that is driven into the power splitter. For this system, a pulse time of 6 μs corresponds to a 90° flip of the magnetization of the sample. The delay between 90° and 180° pulses, known as the tau value, is 0.625 ms. There are 1980 pulses per scan, which results in a total relaxation window of 2.5 s. There is a 10 s relaxation delay between scans to ensure the sample has fully relaxed, so 4 averages of

a sample decay curve take less than a minute. The LabVIEW program is set up to pick out and plot the peak voltage of each spin echo and is plotted vs time, which is modeled by the following:

$$M_{\mathrm{xy}}(t) = M_0 \exp(-R_2 t) \tag{4}$$

where the magnetization at time t is $M_{\mathrm{xy}}(t)$, the initial magnetization is M_0, and R_2 is the transverse relaxation rate.

Fig. 4 shows three spin echos acquired following the application of one 90° and two 180° pulses. A signal-to-noise ratio of 25 dB was measured for a single scan. Although one might expect each successive echo in Fig. 4 to have a smaller amplitude, there tend to be fluctuations in the amplitude of the first few spin echoes in a scan due to phase differences in the 90° and 180° RF pulses and noise in the system. These fluctuations become much less noticeable after a few successive 180° pulses when the phase becomes normalized, and they are reduced even further by averaging multiple scans to build the final decay curve. A graphical user interface (GUI) was created in the front end to set parameters, view the acquired decay curves, and export them for further analysis. The magnetic field strength is affected by a temperature shift gradient of -800 ppm/K, so before a scan, the program must find the optimal operating frequency. After extensive testing at various temperatures, a profile was created to relate the current temperature to the Larmor frequency. A thermocouple is used to measure the ambient temperature, and the correct frequency can be selected based on the known profile.

TABLE I
ASH SAMPLES COLLECTED FROM LNU LIGHTNING COMPLEX FIRE AREA

ash source	date	MP concentration (mg/mL)
structure/residential	10/7/20	0.003
structure/residential	10/7/20	0.006
vehicle	10/7/20	0.008
vehicle	10/7/20	0.008
structure/residential	10/7/20	0.006
structure/residential	10/7/20	0.022
vegetation	10/8/20	0.004
structure/residential	10/15/20	0.016
structure/residential	10/15/20	0.014
structure/residential	10/15/20	0.010
structure/residential/paint	10/15/20	0.016
structure/residential/paint	10/15/20	0.025
structure/vehicle	10/16/20	0.017
structure/vehicle	10/16/20	0.015
vehicle	10/16/20	0.020
structure/residential	10/16/20	0.025

III. MATERIALS & METHODS

A. Ash Sample Collection

The LNU Lightning Complex Fire, which was the sixth largest in California history, destroyed 1491 structures and burned 1470 km^2 of land approximately 60 km west of Sacramento between August 17 and October 2, 2020. The land use within the perimeter of the fire consisted of 1.4% developed, 12% evergreen forest, 19% herbaceous, and 57% shrub/scrub. Ash samples were collected from burned structures, vehicles, and vegetation using disposable plastic scoops and zippered plastic bags prior to any rain or precipitation. The speciation of iron in the fire ash was determined using x-ray absorption spectroscopy. The concentration of magnetic iron was determined using the total iron concentration and the relative abundance of magnetic particles in the fire ash [19]. The ash samples were then prepared for the TD-NMR system by mixing 20 mg of ash with 20 mL of MilliQ (MQ) water and were sonicated and transferred to 5 mm tubes (Norell XR-55). Table I describes the fire ash, including the MP concentration.

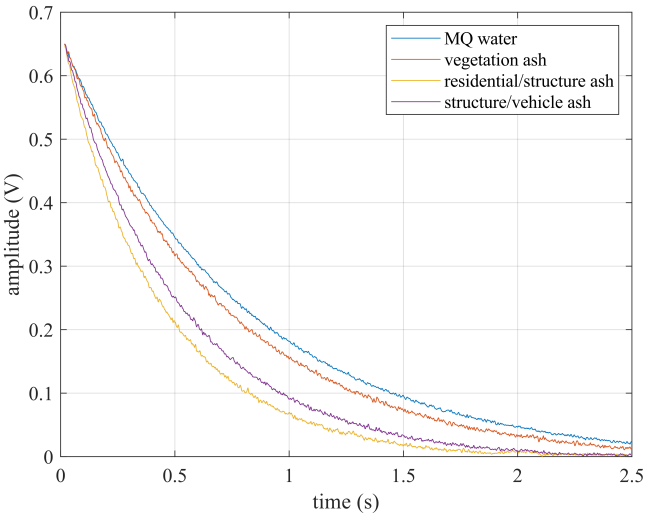

Fig. 5. Results showing transverse relaxation curves for distilled water and three ash samples of varying color and content.

TABLE II
WATER SAMPLES COLLECTED FROM LAKE MADRONE INLETS FOLLOWING FIRE AND RAINFALL EVENTS

location	date	time
north inlet	11/13/20	10:00am
north inlet	11/13/20	4:00pm
north inlet	11/13/20	10:00pm
north inlet	11/14/20	4:00am
north inlet	11/14/20	10:00am
south inlet	11/13/20	11:00am
south inlet	11/13/20	5:00pm
south inlet	11/13/20	11:00pm
south inlet	11/14/20	5:00am
south inlet	11/14/20	11:00am

B. Runoff Sample Collection

Lake Madrone, located in eastern Butte County, CA, was selected as the sample site for this study. It is 0.10 km^2 and surrounded by a gated mountain community along Berry Creek. Water enters from five total drainages, but the most prominent inlets are Martin Creek (north inlet) and Berry Creek (south inlet). The entire town of Berry Creek was destroyed in the North Complex Fire, which was the seventh largest in California history and destroyed 2,455 structures and burned 1290 km^2 of land between August 17 and December 3, 2020 [19]. The samples were collected before and during a rainfall on September 13 and 14 of 2020. Sample collection was carried out at the north inlet (39°38'59.3"N 121°24'9.1"W)

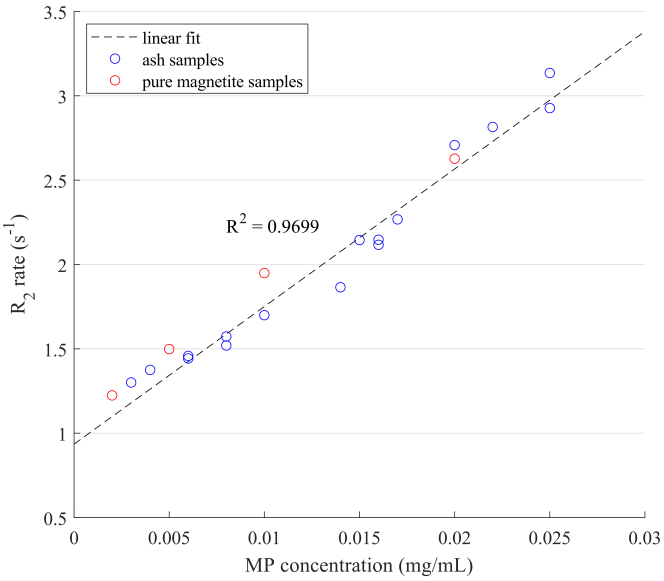

Fig. 6. Results showing the linear correlation of relaxation rate R_2 and MP concentration for pure magnetite and various wildfire ash samples suspended in water.

Fig. 7. Simple MP separator made using a permanent magnet block and a 3D printed housing.

and the south inlet (39°38'40.2"N 121°24'3.8"W) from Martin and Berry Creek before any mixing with water from Lake Madrone. Samples were collected using an autosampler (ISCO 6712, Teledyne, USA). Sample bottles were acid-washed in 10% nitric acid and soaked in ultrahigh purity water for 24 hours each, air dried, and double bagged. Samples were double-bagged individually and returned to the lab the same day to be stored in the dark at 4°C. They were shipped to the University of South Carolina overnight. The location, date, and time for each sample that was collected is shown in Table II.

IV. Results & Discussion

A. Ash & Pure Magnetite Results

To confirm that the TD-NMR system could accurately estimate MP concentrations in fire ash, the system was also used to analyze a set of samples of magnetite suspended in MQ water at concentrations in the range of 0.002 mg/mL to 0.020 mg/mL. These concentrations are within the range of MP concentrations in the fire ash (Table I). The pure magnetite particles ranged from 50-100 nm in size. To determine a basis

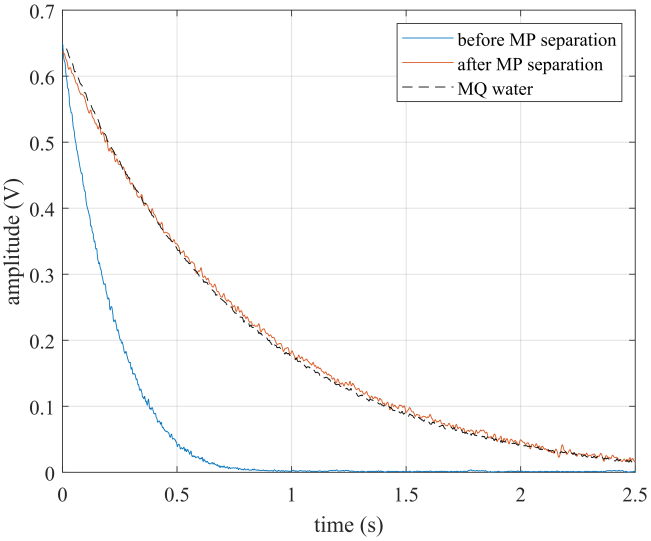

Fig. 8. Results showing transverse decay curves of a runoff sample before and after undergoing MP separation. The decay curve for MQ water is added for reference.

for the relaxation rate with no MPs present, a sample of MQ water was analyzed. It was observed that the nominal relaxation rate for water with no MPs present is about 1.25 s^{-1} in this system. This transverse decay curve, along with curves obtained from a few of the ash samples to show the variance, are plotted in Fig. 5. 16 total ash samples were tested, and their decay rates were extracted via least squares regression according to (1). The R_2 rates for the ash and pure magnetite samples were plotted against the predetermined MP concentrations (in mg/mL) and can be seen in Fig. 6. The linear relationship that was predicted is visible, and the R^2 value (0.9699) of the fit indicates that this technique is a viable method for quickly estimating total MP concentrations in ash. Detection is limited, however, as any concentration lower than 0.001 mg/mL has effects on the relaxation rate that are too negligible to accurately quantify with this system.

B. Magnetic Particle Separator

In order to verify that the system can quantify MP concentrations in surface water, a test was conducted using a rudimentary magnetic particle separator. This was done to ensure that any changes in relaxation rate were solely due to the presence of MPs and not caused by unknown variables in the water samples. This tool, shown in Fig. 7, consists of an N42 permanent magnet block placed within a 3D printed frame with slots for inserting centrifuge tubes. When a sample tube is placed in it, the MPs in the suspension will be drawn toward the magnet and will concentrate on the wall of the tube closest to the magnet. Water can then be extracted from the tube at the wall opposite the magnet to ensure that there is no magnetic content remaining. A surface water sample was selected that displayed a high R_2 value compared to distilled water, and it was placed in the device to be left overnight. After having ample time to undergo magnetic separation, water was extracted from the tube as described and tested once again

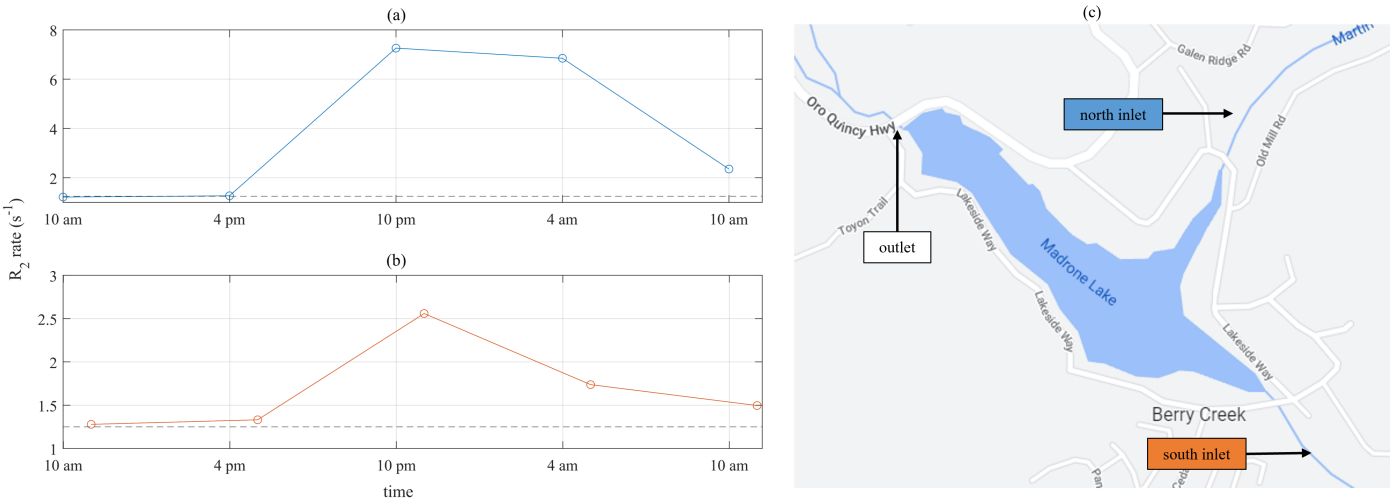

Fig. 9. Results of runoff water testing showing R_2 rates measured over both campaigns for the: (a) north inlet (b) and south inlet of Lake Madrone. The dotted line in each figure represents the R_2 rate for pure distilled water. (c) is a map of the locations where samples were obtained at each inlet.

with the TD-NMR system. Results from before and after the particle separation, as well as distilled water for reference, are shown in Fig. 8 and confirm the expected result. The relaxation rate returned to the nominal value, so it can be concluded that increases in relaxation rate observed in surface water samples are caused by MP presence.

C. Runoff Water Results

To extend the usefulness of the TD-NMR system to the possibility of in situ monitoring of MPs in natural water bodies, the analysis was conducted on the samples of water obtained from Lake Madrone in California following the North Complex Fire in September of 2020. To see if the TD-NMR system is able to observe increases in R_2 rates over time for the samples reported in Table II, water from each sample was transferred into a 5 mm NMR tube, tested, and the decay rates were extracted as described before. The results are presented in Fig. 9 along with a map indicating the locations that the samples were taken from. An R_2 value around 1.25 s^{-1}, represented by a horizontal dashed line in Fig. 9(a) and Fig. 9(b) means that the system detected little MP presence in the sample. The plots show that the relaxation rates increased during the rainfall event before eventually decreasing back to the steady state value. The spike in relaxation rates during the rainfall period indicates the viability of the system as a tool for in situ monitoring of MP presence over time in natural bodies of water. The recorded R_2 values could also be converted to an equivalent concentration of magnetite particles using the known linear relationship to give an estimate of the concentration of MPs in the water.

V. Conclusion

This work demonstrates the ability to construct an environmental sensor for monitoring MP concentrations in wildfire ashes and natural water impacted by runoff from burned areas using TD-NMR. This system employs a compact, low-cost permanent magnet design that produces a sufficiently strong and homogeneous field to achieve clear results for NMR relaxometry. The custom electronics and subsystems required to route and amplify excitation and detection signals were shown, along with the controls and used to accomplish the timing and data acquisition. This system demonstrates a quick and simple method for estimating the concentration of MPs in wildfire ashes suspended in water, and can also be used to monitor magnetic content levels in surface water and MPs discharged from other combustion processes such as releases from coal ash ponds or urban runoff. A device such as this could be immensely useful in determining how widespread the effects of a wildfire are and can be used as a proxy for the discharge of ashes from wildfires, coal ash ponds, and other sources. Environmental factors such as ambient temperature can affect the operation of the system. A temperature shift of 17 K from the originally tuned temperature would require the probe to be recalibrated. This calibration is currently manual, but an auto-tuning function is very feasible to implement. On the other hand, the temperature of the magnet could be regulated using insulating material or a Peltier cooler to curb fluctuations. Although it would consume some significant extra power, a prototype temperature regulation chamber with a Peltier cooler has been tested in the lab and is effective for maintaining the magnet temperature to 2 K of fluctuation. The circuitry must also be tightly sealed when placed outdoors to prevent any moisture or rain from causing damage. Future work will be dedicated to further improving the size, portability, and energy consumption of the TD-NMR system so that it can be deployed for extended times for in situ monitoring of MPs in water and soil.

VI. Acknowledgment

We would like to thank Jackson P. Webster (Department of Civil Engineering, California State University Chico), Sandrine Matiasek (Department of Earth and Environmental Sciences, California State University Chico), and Charles N.

Alpers (U.S. Geological Survey, California Water Science Center) for their help with sample collection and data logging.

REFERENCES

[1] J. Martin, A. R. Downey, M. Baalousha, and S. H. Won, "Measurement of magnetic particle concentrations in wildfire ash via compact nmr," in *2022 IEEE Sensors*, 2022, pp. 1–4.

[2] K. Hatada and T. Kitayama, *Introduction to NMR Spectroscopy*. Berlin, Heidelberg: Springer Berlin Heidelberg, 2004, pp. 1–42. [Online]. Available: https://doi.org/10.1007/978-3-662-08982-8_1

[3] M. K. Singh and A. Singh, "Chapter 14 - nuclear magnetic resonance spectroscopy," in *Characterization of Polymers and Fibres*, ser. The Textile Institute Book Series, M. K. Singh and A. Singh, Eds. Woodhead Publishing, 2022, pp. 321–339. [Online]. Available: https://www.sciencedirect.com/science/article/pii/B9780128239865000117

[4] F. A. Nelson and H. E. Weaver, "Nuclear magnetic resonance spectroscopy in superconducting magnetic fields," *Science*, vol. 146, no. 3641, pp. 223–232, 1964. [Online]. Available: https://www.science.org/doi/abs/10.1126/science.146.3641.223

[5] J. Fattori, F. H. Rodrigues, J. G. Pontes, A. Paula Espíndola, and L. Tasic, "Chapter 6 - monitoring intermolecular and intramolecular interactions by nmr spectroscopy," in *Applications of NMR Spectroscopy: Volume 3*, A. ur Rahman and M. I. Choudhary, Eds. Bentham Science Publishers, 2015, pp. 180–266. [Online]. Available: https://www.sciencedirect.com/science/article/pii/B9781681080635500060

[6] A. G. Abdul Jameel, V. Van Oudenhoven, A.-H. Emwas, and S. M. Sarathy, "Predicting octane number using nuclear magnetic resonance spectroscopy and artificial neural networks," *Energy & Fuels*, vol. 32, no. 5, pp. 6309–6329, 2018. [Online]. Available: https://doi.org/10.1021/acs.energyfuels.8b00556

[7] B. Blümich, "Low-field and benchtop nmr," *Journal of Magnetic Resonance*, vol. 306, pp. 27–35, 2019. [Online]. Available: https://www.sciencedirect.com/science/article/pii/S1090780719301594

[8] S. S. Zalesskiy, E. Danieli, B. Blümich, and V. P. Ananikov, "Miniaturization of nmr systems: Desktop spectrometers, microcoil spectroscopy, and "nmr on a chip" for chemistry, biochemistry, and industry," *Chemical Reviews*, vol. 114, no. 11, pp. 5641–5694, Jun 2014. [Online]. Available: https://doi.org/10.1021/cr400063g

[9] L. E. Marbella and J. E. Millstone, "Nmr techniques for noble metal nanoparticles," *Chemistry of Materials*, vol. 27, no. 8, pp. 2721–2739, 2015. [Online]. Available: https://doi.org/10.1021/cm504809c

[10] Y.-T. Chen, A. G. Kolhatkar, O. Zenasni, S. Xu, and T. R. Lee, "Biosensing using magnetic particle detection techniques," *Sensors*, vol. 17, no. 10, 2017. [Online]. Available: https://www.mdpi.com/1424-8220/17/10/2300

[11] H. Shao, T.-J. Yoon, M. Liong, R. Weissleder, and H. Lee, "Magnetic nanoparticles for biomedical NMR-based diagnostics," *Beilstein J Nanotechnol*, vol. 1, pp. 142–154, Dec. 2010.

[12] N. Sun, T.-J. Yoon, H. Lee, W. Andress, R. Weissleder, and D. Ham, "Palm nmr and 1-chip nmr," *IEEE Journal of Solid-State Circuits*, vol. 46, no. 1, pp. 342–352, 2011.

[13] J. Gunn, R. K. Paranji, and M. Zhang, "A simple and highly sensitive method for magnetic nanoparticle quantitation using 1H-NMR spectroscopy," *Biophys J*, vol. 97, no. 9, pp. 2640–2647, Nov. 2009.

[14] A. S. Minin, M. A. Uymin, A. Y. Yermakov, I. V. Byzov, A. A. Mysik, M. B. Rayev, P. V. Khramtsov, S. V. Zhakov, A. V. Volegov, and I. V. Zubarev, "Application of NMR for quantification of magnetic nanoparticles and development of paper-based assay," *Journal of Physics: Conference Series*, vol. 1389, no. 1, p. 012069, nov 2019. [Online]. Available: https://doi.org/10.1088/1742-6596/1389/1/012069

[15] S. L. Reneau, D. Katzman, G. A. Kuyumjian, A. Lavine, and D. V. Malmon, "Sediment delivery after a wildfire," *Geology*, vol. 35, no. 2, pp. 151–154, 02 2007. [Online]. Available: https://doi.org/10.1130/G23288A.1

[16] E. National Academies of Sciences and Medicine, *The Chemistry of Fires at the Wildland-Urban Interface*. Washington, DC: The National Academies Press, 2022. [Online]. Available: https://nap.nationalacademies.org/catalog/26460/the-chemistry-of-fires-at-the-wildland-urban-interface

[17] M. Alam, T. Alshehri, J. Wang, S. A. Singerling, C. N. Alpers, and M. Baalousha, "Identification and quantification of cr, cu, and as incidental nanomaterials derived from cca-treated wood in wildland-urban interface fire ashes," *Journal of Hazardous Materials*, vol. 445, p. 130608, 2023. [Online]. Available: https://www.sciencedirect.com/science/article/pii/S0304389422024025

[18] T. Alshehri, J. Wang, S. A. Singerling, J. Gigault, J. P. Webster, S. J. Matiasek, C. N. Alpers, and M. Baalousha, "Wildland-urban interface fire ashes as a major source of incidental nanomaterials," *Journal of Hazardous Materials*, vol. 443, p. 130311, 2023. [Online]. Available: https://www.sciencedirect.com/science/article/pii/S0304389422021057

[19] M. Baalousha, M. Desmau, S. A. Singerling, J. P. Webster, S. J. Matiasek, M. A. Stern, and C. N. Alpers, "Discovery and potential ramifications of reduced iron-bearing nanoparticles—magnetite, wüstite, and zero-valent iron—in wildland–urban interface fire ashes," *Environ. Sci.: Nano*, vol. 9, pp. 4136–4149, 2022. [Online]. Available: http://dx.doi.org/10.1039/D2EN00439A

[20] J. L. Till, B. Moskowitz, and S. W. Poulton, "Magnetic properties of plant ashes and their influence on magnetic signatures of fire in soils," *Frontiers in Earth Science*, vol. 8, 2021. [Online]. Available: https://www.frontiersin.org/article/10.3389/feart.2020.592659

[21] N. Jordanova, D. Jordanova, and V. Barrón, "Wildfire severity and its environmental effects revealed by soil magnetic properties," *Land Degradation & Development*, vol. 30, 07 2019.

[22] H. Y. Carr and E. M. Purcell, "Effects of diffusion on free precession in nuclear magnetic resonance experiments," *Phys. Rev.*, vol. 94, pp. 630–638, May 1954. [Online]. Available: https://link.aps.org/doi/10.1103/PhysRev.94.630

[23] A. Louis-Joseph and P. Lesot, "Designing and building a low-cost portable ft-nmr spectrometer in 2019: A modern challenge," *Comptes Rendus Chimie*, vol. 22, no. 9, pp. 695–711, 2019. [Online]. Available: https://www.sciencedirect.com/science/article/pii/S1631074819301055

[24] E. I. GREEN, "The story of q," *American Scientist*, vol. 43, no. 4, pp. 584–594, 1955. [Online]. Available: http://www.jstor.org/stable/27826701

[25] B. Blümich, "Introduction to compact nmr: A review of methods," *TrAC Trends in Analytical Chemistry*, vol. 83, pp. 2–11, 2016, sI: Compact NMR. [Online]. Available: https://www.sciencedirect.com/science/article/pii/S0165993615301886

[26] G. Moresi and R. Magin, "Miniature permanent magnet for table-top nmr," *Concepts in Magnetic Resonance Part B: Magnetic Resonance Engineering*, vol. 19B, no. 1, pp. 35–43, 2003. [Online]. Available: https://onlinelibrary.wiley.com/doi/abs/10.1002/cmr.b.10082

[27] B. Blümich, C. Rehorn, and W. Zia, *Magnets for Small-Scale and Portable NMR*. John Wiley & Sons, Ltd, 2018, ch. 1, pp. 1–20. [Online]. Available: https://onlinelibrary.wiley.com/doi/abs/10.1002/9783527697281.ch1

[28] D. Meeker, "Finite element method magnetics," *FEMM*, vol. 4, no. 32, p. 162, 2010.

[29] *Compact Time Domain NMR Design for the Determination of Hydrogen Content in Gas Turbine Fuels*, ser. International Design Engineering Technical Conferences and Computers and Information in Engineering Conference, vol. Volume 1: 24th International Conference on Advanced Vehicle Technologies (AVT), 08 2022, v001T01A017. [Online]. Available: https://doi.org/10.1115/DETC2022-90023

[30] T. D. Claridge, "Chapter 3 - practical aspects of high-resolution nmr," in *High-Resolution NMR Techniques in Organic Chemistry (Third Edition)*, third edition ed., T. D. Claridge, Ed. Boston: Elsevier, 2016, pp. 61–132. [Online]. Available: https://www.sciencedirect.com/science/article/pii/B9780080999869000038

Jacob S. Martin is currently a graduate research assistant in the Adaptive Real Time Systems Laboratory (ARTS) Lab at the University of South Carolina, where he is pursuing a M.S. in Physics. He obtained a B.S. in electrical engineering from the University of South Carolina in 2021. He first worked as an intern in the engineering division of Wieland copper in North Carolina, and has gone on to hold positions in the Department of Defense, one at Naval Information Warfare Center (NIWC) Atlantic, and one at the Joint Warfare Analysis Center (JWAC). His graduate research has been focused on the development of a tabletop nuclear magnetic resonance (NMR) system for fuel and environmental analysis, which has been the subject of two published conference papers. He continues to work collaboratively with the Mechanical Engineering department, the Arnold School of Public Health, and the Physics & Astronomy department on various projects involving magnetic particle spectroscopy, piezoelectric plasma generation, permanent magnet design, and RF communication systems.

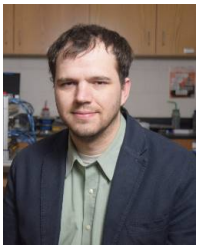

Austin Downey Dr. Austin Downey is an Assistant Professor of Mechanical Engineering for the College of Engineering and Computing at the University of South Carolina. He received a B.S. in Civil Engineering and a Ph.D. in Engineering Mechanics; and Wind Energy Science, Engineering, and Policy (dual majors) from Iowa State University, USA. His expertise and research interest include in situ sensing, low-latency machine learning, and adaptive structures.

Mohammed Baalousha Dr. Mohammed Baalousha is a Professor of Environmental Nanoscience at the University of South Carolina. He obtained a BSc in Civil Engineering from the Islamic University of Gaza, Palestine, a Masters in Applied Mechanics and a Ph.D. in Environmental Biogeochemistry from the University of Bordeaux, France. He also has undertaken a variety of postdoctoral research roles at the University of Birmingham, United Kingdom in the area of Environmental Nanoscience. Dr. Baalousha's research interests are interdisciplinary in nature and are centered on the understanding of the sources, measurements, transformations, fate, applications, and environmental implications of natural, engineered, and incidental nanomaterials.

Sang Hee Won Dr. Sang Hee Won is an Associate Professor of Mechanical Engineering and Interim Director of Aerospace Engineering for the College of Engineering and Computing at the University of South Carolina. He obtained a B.S. in Mechanical Engineering, a M.S. in Mechanical Engineering, and a Ph.D. in Mechanical and Aerospace Engineering from Seoul National University, South Korea. Dr. Won's research involves; 1) Combustion chemistry of real transportation fuels with the state-of-the-art current kinetic models to incorporate multi-species combustion chemistry, 2) Development of well-defined experimental platforms to investigate the role of combustion chemistry in near-limit combustion dynamics, where complicated turbulent-chemistry interactions can be fundamentally investigated, 3) Plasma-assisted combustion techniques, in which the near-limit combustion dynamics are manipulated by plasma, will be introduced based on the understanding of combustion chemistry, and 4) Development of novel combustion diagnostic techniques.